Corrosion behavior of 316L stainless steel coatings on ZE41 magnesium alloy in chloride environments

S. García-Rodríguez, B. Torres, N. Pulido-González, E. Otero, J. Rams*

Área de Ciencia e Ingeniería de Materiales, ESCET, Universidad Rey Juan Carlos *C/ Tulipán s/n, Móstoles 28933 Madrid (Spain)*

Abstract

The corrosion behavior of the ZE41 magnesium alloy with a HVOF 316L stainless steel coating was electrochemically evaluated in 3.5 wt.% NaCl solution and by salt spray testing. Electrochemical Impedance Spectroscopy (EIS) allowed determining the resistance of the coatings deposited, the growth of compact corrosion products on the ZE41 Mg alloy and the failure of the non-optimized coatings. The best coating resisted the chloride attack for long times in immersion and in salt spray environments, and it drastically reduced galvanic couple formation. Its behavior is associated with its reduced porosity and its higher compactness and mechanical stability.

Keywords: *HVOF; Magnesium; metal coatings; stainless steel; EIS;*

*corresponding author:
Prof. Joaquin Rams
joaquin.rams@urjc.es

1. Introduction

In the automotive, aeronautic, electronic and military industry, magnesium alloys stand out as a promising alternative to Al alloys or steels with the aim to reduce the weight of the vehicles, and, moreover, to improve fuel economy. Mg alloys are the lightest of all metals used as the basis for constructional alloys, they have high strength to weight ratio and excellent electromagnetic shielding characteristics [1,2]. The ZE41 magnesium alloy is particularly attractive to the industry due to its adequate mechanical properties (damping capacity, impact resistance and dimensional stability, among others) at room and at elevated temperatures due to solution and precipitation hardening treatments [3]. However, the use of this alloy, like most magnesium alloys, is limited due to their insufficient surface properties, particularly their poor wear and corrosion resistance. The most severe challenge of the application of Mg alloys is to solve the problem of their inferior corrosion resistance caused by the chemical activity of Mg [4,5], especially in aggressive environments [3–6], such as in presence of chloride. In the "mixed-construction" applications that implies the contact between different materials, the disadvantages of the use of magnesium alloys increase due to the galvanic corrosion. The contact between noble components, such steel, and Mg in, for example, saltwater, generate a difference in potential causing a galvanic corrosion [7].

To improve the corrosion behavior of Mg alloys different surface treatments have been developed such us chemical conversion treatments [8], sol-gel silica coatings [9], laser surface melting [10], magnetron sputtering [11] or thermal spray coatings [12], being this last one the most effective way to improve the surface behavior of most materials. Using the High Velocity Oxygen-Fuel (HVOF) spraying technique, hard, dense and low-porosity coatings can be developed in a high variety of substrates and it allows depositing many different materials. They are considerer the best coatings against corrosion due to the high porosity generated by other thermal spray technique limits their useful [13–15].

In the HVOF spraying process the powder material is melted or semi-melted and propelled at high speed on the surface of the substrate. To achieve this, a combustion generated by a mixture of gases and oxygen is used. The high volume of gases and the high temperature reach by the combustion leads to obtain pressures above 241 kPa and gas speeds greater than 2000 m/s [16]. The spraying powder is fed into the generated flame spray using a transport gas. Thus, the powder particles are melted or semi-melted, depending on the temperature of the flame, and sprayed at high speed. Particles with sizes between 10 and 63 µm can reach velocities between 300 and 800 m/s [17].

Among the alternatives available, stainless steel (SS) appears on as a suitable one as it is a reference material for wear, corrosion and mechanical properties. Moreover, stainless steel coatings manufactured by HVOF provided an alternative to protect components against corrosion in different aggressive environments, due to they are dense and exhibit low oxidation in compared with coatings obtained by other thermal spray techniques such us plasma or wire arc spray [18,19]. Guilemany et al. [20] studied the corrosion behavior of the stainless steel coating manufactured by HVOF on steel substrate. They observed that the spraying parameters such us gun transverse speed, spray distance and gas flow strongly influence the corrosion resistance of these coatings, showing that using higher spraying distance the obtained coating had better protective properties in NaCl solution. Corrosion behavior of 316L stainless steel coating manufactured using different spraying techniques in different acidic solutions were also studied in [21]. They observed that coatings manufactured by HVOF had low oxidation, were harder and showed better corrosion behavior than the coatings manufactured by atmospheric plasma spray or shrouded plasma spray.

In addition to Direct Current technique (DC) (potentiodynamic polarization), the Alternate Current (AC) impedance allows monitoring the corrosion behavior of a variety of systems (metals, alloys, metals coated, metal matrix composites, etc.) [22–25]. This technique provides

important information about surface layers grown on coated metals and the interface between films/coatings and substrates. With the analysis of the Electrochemical Impedance Spectroscopy (EIS) parameters it is possible to obtain corrosion mechanisms and fundamental parameters related to electrochemical kinetics [26,27].

In a previous study [28], we optimized the spraying parameters (spraying distance, spraying speed and gas mixture) in order to deposit 316L stainless steel on a ZE41 magnesium alloy. The coatings showed high hardness and provided some corrosion protection to the substrate, as it was evaluated by potentiodynamic tests. In this paper, 316L stainless steel coatings deposited by HVOF on ZE41 magnesium alloys have been also tested. The spraying conditions used were the same than those shown in ref [28] but the number of layers was varied. In addition, a deeper study of the corrosion behavior of these coatings in chloride environments using chloride salt spray and chloride solution in a real system have been proven to be crucial for enhancing the system reliability. EIS analysis and the galvanic corrosion test complete the novelty of this the study with obtaining the resistance of the different barriers that suppose the incorporation of the different coatings.

2. Experimental procedure

2.1. Materials

Extruded rods of ZE41 cast alloy, supplied by Magnesium Elektron Company, with a nominal composition (wt.%) of: 4.09 Zn; 1.7 rare earths (Pr + Nd + La + Ce); 0.68 Zr; 0.6 O; and balance Mg, were used as substrates. The material was received with the aging treatment T5 (2h at 330 ^{o}C followed by 10 – 16 h at 177 ^{o}C). The rod was cut in 10 mm thick and 60 mm diameter discs. The samples were sand blasted with 1 mm corundum particles, ultrasonically cleaned in ethanol and air-dried before spraying.

Austenitic stainless steel powder provided by Sulzer-Metco (Diamalloy 1003), similar to 316L stainless steel, was used as feedstock in the thermal spray process. The particle size

distribution of the stainless steel powder was -45 + 11 µm and its nominal composition was (wt.%): 17 Cr, 12 Ni, 2.5 Mo, 2.3 Si, 0.03 C and balance Fe.

2.2. Spraying process

Stainless steel coatings were manufactured by a High Velocity Oxygen-Fuel thermal spraying (HVOF) equipment from Sulzer Metco (Unicoat, DS2600) placed on an ABB IRB-2400/16 robot that mixed oxygen (147 NLPM - normalized liter per minute) with hydrogen (717 NLPM), air as shielding gas (438 NLPM) and nitrogen as transport gas.

The spraying conditions were: spraying distance of 300 mm, gun speed of 250 mm/s, 4, 3, 2 or 1 layers (SS4, SS3, SS2 and SS1 respectively) and a feeding rate of powder to the gun of 26 g/min. These conditions were previously optimized.

2.3. Specimen examination

The morphological features of the coatings were analyzed on the cross-section by Scanning Electron Microscopy (SEM, Hitachi S-3400N) equipped with an Energy Dispersive X-Ray Spectrometer (EDS, XFlash 5010 Brukert). For microscopic characterization, metallographic samples were cut using a SiC disc cutter, hot mounted in conductive resin, ground with SiC emery paper up to 4000 grade and polished with diamond paste to 1 µm.

To complete the microstructural characterization of the samples and to measure the porosity and the oxide content of the coatings, light microscopy (Leica DMR) with Leica Image Proplus image analysis software was used.

Microhardness across the coatings was measured on the cross-sections using SIHMADZU HMV-2 microhardness tester applying 980.7 mN (HV0.1). The results are the average of at least three indentation tests.

The adhesion strengths between coatings and substrates were evaluated by a tensile test using a Posi-Test At-Pull-Off Adhesion Tester, following the ASTM D4541-02 procedure [29].

2.4. Salt spray environment

Samples were placed in a salt spray chamber exposed to a 50 g/l NaCl spray in a pH solution of 7.1 - 7.2. Atomized air pressure of the saline solution was maintained at 1.2 bar, following the UNE-EN ISO 9227:2012. The temperature inside the chamber was 35 ^{o}C.

Exposure times up to 72 h have been used. The sample area exposed to the salt spray environment was 2.25 cm^2 for all samples tested and the rest of the sample was covered with resin. Three samples for each coating condition were tested.

2.5. Electrochemical measurements

Corrosion behavior of the different specimens was evaluated at room temperature in 3.5 wt.% NaCl with an Autolab PGStat302N potentiostat, provided with Nova 2.1 software. Measurements were carried out using a conventional three-electrode cell configuration with a graphite rod counter electrode, a silver/silver chloride (Ag/AgCl, KCl 3M) as a reference electrode and the coated samples as the working electrode. The coated surface was pressed against an opening in the electrochemical cell with a rubber O-ring, exposing only an area of 0.76 cm^2 of the coated surface to the electrolyte.

2.5.1. Potentiodynamic polarization studies

To obtain the polarization resistance of the samples (*Rp*), linear polarization tests were carried out varying the potential from ±10 mV around the corrosion potential (E_{corr}), using a 1 mV/s scanning rate. The *Rp* values were evaluated for each sample after different immersion times in the electrolyte solution (1, 6, 24, 48, 72, 96 and 168 h) in order to study the evolution of the coating protection with time.

Tafel curves (the anodic-cathodic polarization measurements) were carried out by polarizing between -400 to 800 mV around the corrosion potential with a scanning rate of 1 mV/s. Before starting the test, a time for the stabilization of the open circuit potential (OCP) was expected.

2.5.2. Electrochemical Impedance Spectroscopy (EIS)

AC Electrochemical Impedance measurements were carried out by applying a sinusoidal potential wave at E_{corr} with an amplitude of 10 mV over the frequency range from 10^5 to 10^{-2} Hz, recording 10 points per decade. The impedance data were analyzed using Nyquist and Bode plots.

EIS test were performed at immersion times of 1, 6, 24, 48 and 144 h in the 3.5 wt.% NaCl electrolytic solution. All the electrochemical tests were performed in duplicate to examine the reproducibility of the results.

2.5.3. Galvanic corrosion resistance

To study the galvanic corrosion resistance when this coated system is in contact with a galvanized iron screw (simulating a real system), the coated samples were attached with another metal in a system as shown in Figure 1. In this system, the stainless steel coating was in contact with a galvanized iron screw.

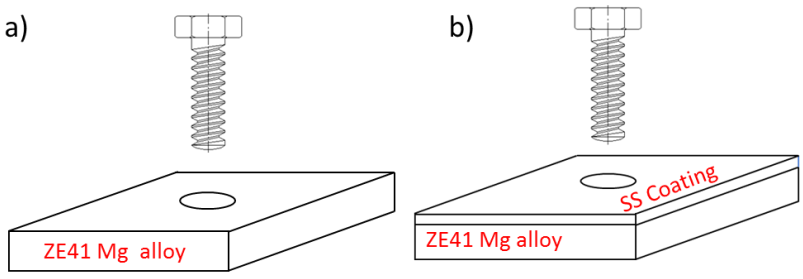

Figure 1. a) ZE41 magnesium alloy and b) stainless steel coating both attached with galvanized iron bolt.

A 5 mm diameter hole was made in all samples tested. The screw area which is in contact with the magnesium alloy (inside the hole) was covered with Teflon to avoid the penetration of the solution. Moreover, galvanic current was measured by immersing the bolt and the coated samples in the solution.

3. Results and discussion

3.1. Microstructure of the HVOF coatings

Figure 2 shows the cross-sections of the SS1, SS2, SS3 and SS4 sprayed coatings. All coatings were dense, continuous, free from cracks and well adhered, with values higher than 32 MPa (the maximum value resisted by the adhesive). Some porosity was observed in the most external layer of the coating (marked by arrow in Figures 2b and 2c), but its amount was negligible (< 0.1%), which is much lower than the results obtained by other authors who have used HVOF on substrates that were harder than magnesium [30]. The main characteristics of the coatings are shown in Table 2. The thickness of the coatings increased as the number of deposited layers increases, but similar values were obtained when the number of layers increased from 3 to 4 layers. However, mass gain in the coating increased as the number of sprayed layers also did, being higher for the SS4 sample. These both features suggest that the impact of particles on previously deposited layers generates very dense coatings, and its compactness increases with the number of deposited layers [31]. This effect prevented the presence of porosity in the inner part of the coatings and, moreover, resulted in an important increase of the hardness values obtained for each sample, being harder for the thickest coating (SS4) (433 ± 35 HV for SS4 and 328 ± 25 HV for SS1). In a previous work [32] we observed that in each layer the sprayed particles are molten and quenched on the substrate, but their impact on previous layers also induce plastic deformation of them, and even on the substrate, so a peening stress was introduced (compressive component). This deposited layer also induces a

heat treatment on the deposited coating. Finally, when the system cools to room temperature, a thermal stress appears due to the difference in the coefficients of thermal expansion between the coating and the substrate and to the different temperatures reached in them. All this synergistically caused a strong increase in the hardness of these coatings, in special in the 4-layers coating, which were nearly double that of standard 316L SS.

The analysis of the transversal section of the coatings also evidenced that the coatings were mostly constituted by splats. During the spraying process, the stainless steel particles fly in a semi-melted state that deform upon impacting with the samples, but also unmelted particles were observed in the coating. Oxides in the coating appeared as dark grey areas between layers (marked by arrows in Figure 2d) and surrounding semi-melted particles (Figure 2e). The composition of both types of oxides, previously characterized in [28], was similar and they were mainly constituted by α-Fe_2O_3, NiO and Cr_2O_5. Its proportion was similar for all coatings and lower than that obtained by other authors, as most of them have above 10% of oxides in the coating [33] while these below 5.5% (value obtained for SS4).

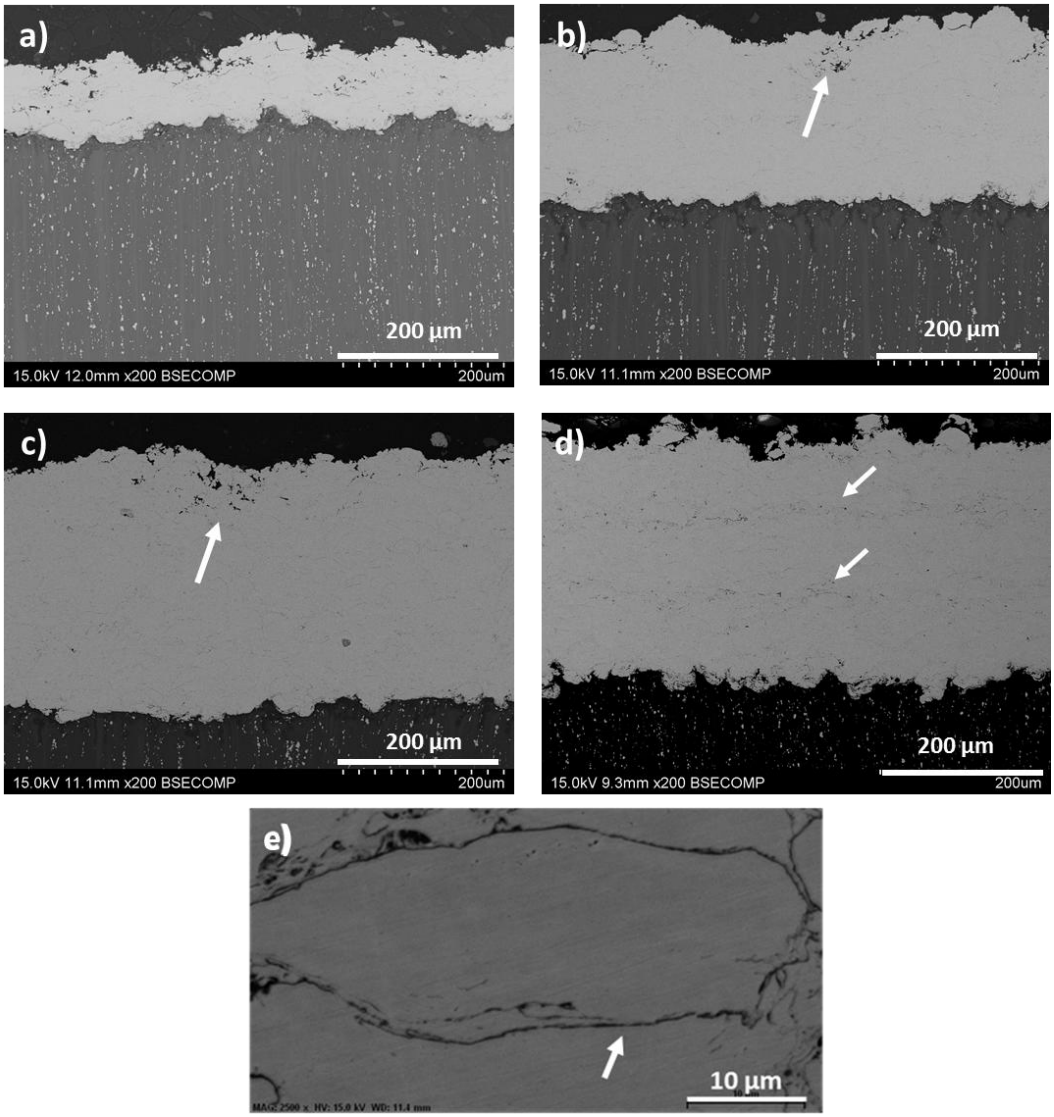

Figure 2. SEM micrographs of coatings a) SS1, b) SS2, c) SS3, d) SS4 and e) semi-melted particle.

Table 2. Morphological and mechanical features of the coatings

Sample	Thickness (µm)	Δm/area (g/cm^2)	Oxide content (vol.%)	Hardness ($HV_{0.1}$)
SS1	100 ± 18	0.039 ± 0.007	4.9 ± 0.8	328 ± 25
SS2	240 ± 13	0.110 ± 0.009	5.1 ± 0.9	349 ± 29
SS3	309 ± 18	0.180 ± 0.010	4.3 ± 0.9	392 ± 31
SS4	318 ± 19	0.260 ± 0.016	5.4 ± 0.6	433 ± 35

3.2. Potentiodynamic polarization measurements

Polarization measurements of ZE41, SS4, SS3, SS2 and SS1 samples were carried out in 3.5 wt.% NaCl. Figure 3a shows the anodic-cathodic curves for the corrosion of the ZE41 magnesium alloy and for all coated samples in 3.5 wt.% NaCl aqueous solution after 1 h of stabilization, and table 3 shows the Open Circuit Potential (OCP) and corrosion current densities (i_{corr}) obtained. In general, the corrosion current density (i_{corr}) is indicative of the corrosion kinetics and the corrosion potential (E_{corr}) is indicative of the thermodynamic characteristics of the reaction systems. The OCP increased when the number of layers increased and, for all coated samples, the value was greater than that of ZE41 magnesium alloy. For the current density, the value decreased when increasing the number of layers. For SS2, SS3 and SS4 samples a lower current density than that of the ZE41 magnesium alloy was obtained and for SS1 the value was greater. The OCP of SS1 coated sample was -1.01 V and it was higher than the value obtained for ZE41 magnesium alloy (-1.48 V). However, the current density of SS1 was much greater than for ZE41 (93.0 μA/cm^2 and 17.9 μA/cm^2, respectively). This is caused by a difference in the corrosion mechanism [28]. Due to the porosity in the unique layer of SS1 sample, the chlorides of the electrolyte easily reach the substrate-coating interface, producing the dissolution of the magnesium substrate and the corrosion process is accelerated due to the formation of a galvanic couple between magnesium (which acts as anode) and stainless steel coating (cathode).

Open circuit potential values for SS2 and SS3 samples (-0.96 V and -0.89V, respectively) were higher than the values of ZE41 and SS1. Both showed lower corrosion current density (9.5 μA/cm^2 and 7.7 μA/cm^2, respectively) than ZE41, so, at immersion time of 1h, both coatings acted as a good corrosion barrier for ZE41 magnesium alloy.

The OCP of SS4 coated sample was -0.19 V. This value was greater than the OCP obtained for the ZE41 magnesium and for all other tested samples, and similar to that of the 316L SS bulk material (-0.20 V) used as a reference. The low current density obtained for this sample

(4.62 µA/cm^2) as compared with the value obtained for the bare ZE41 (17.9 µA/cm^2) evidence the effectiveness of this coating as a protective barrier against corrosion for magnesium alloy.

Figure 3b shows the evolution of the polarization resistance values (*Rp*) of the different systems with immersion time. The lowest *Rp* value was obtained for the ZE41 magnesium alloy after 1 h in NaCl 3.5 % wt. The *Rp* value for the uncoated alloy after 1 h of immersion was 61.06 Ω·cm^2. At this time, the results obtained for the coated samples were greater than that, being 101.24 Ω·cm^2, 91.69 Ω·cm^2, 693.49 Ω·cm^2 and 33560 Ω·cm^2 for SS1, SS2, SS3 and SS4, respectively. The SS1 and SS2 were only recorded until 24 h of immersion time and SS3 until 48 h because, after this time, the detachment of the coating occurred. All the *Rp* values decreased with the increase of the immersion time. After 168 h in 3.5 wt.% NaCl, the *Rp* value of the SS4 sample decreased to 2482 Ω·cm^2. The inset in figure 3b shows the *Rp* results of ZE41, which increases with the immersion time. This *Rp* values evolution indicates that different corrosion mechanisms were taking place in the coated samples than in the Mg alloy. The oxides that grew on the surface of magnesium alloy partially block the attacked zones, slowing down the corrosion evolution and causing a slight increase of the polarization resistance with the immersion time.

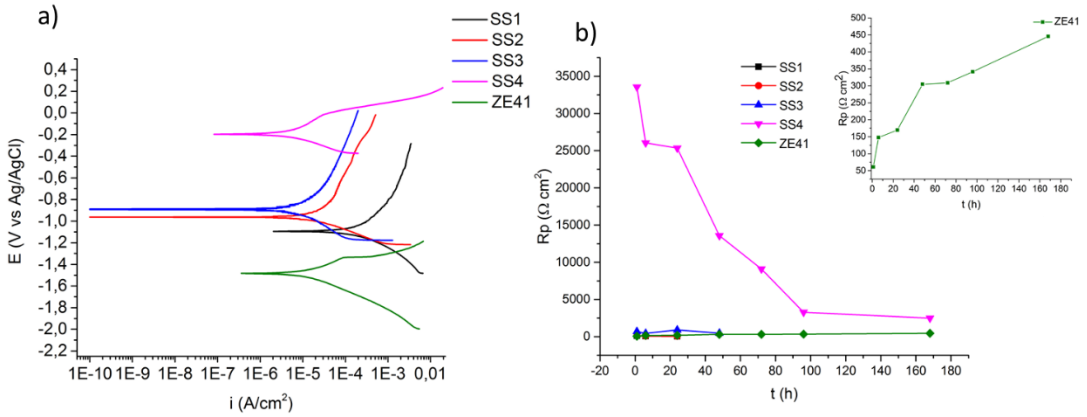

Figure 3. Electrochemical results of the different specimens in 3.5 wt.% NaCl solution a) polarization curves after 1 h immersion b) polarization resistance (*Rp*) vs immersion time.

Table 3. Open Circuit Potential (OCP) and corrosion densities (i_{corr}) of the specimens tested in 3.5 wt.% NaCl aqueous electrolyte obtained of the anodic-cathodic corrosion test after 1h immersion.

Sample	OCP (V)	i_{corr} (μA/cm^2)
ZE41	-1.48 ± 0.08	17.9 ± 5.6
SS1	-1.01 ± 0.07	93.0 ± 9.1
SS2	-0.96 ± 0.03	9.5 ± 1.1
SS3	-0.89 ± 0.01	7.7 ± 0.9
SS4	-0.19 ± 0.02	4.6 ± 0.2

3.3. Salt spray

All samples were exposed to simulated salt spray environment for 72 h on a 2.25 cm^2 area. The morphology of the surface for each sample before and after the test is shown in Figure 4. Three samples for each coating condition have been tested and the most damaged sample has been shown for each exposure time in Figure 4. As shown for SS3 and SS4 specimens the stainless steel coating remains undamaged so the coatings protect the magnesium corrosion during the first 24 h. This does not occur in SS1 and SS2, where some corrosion products appeared on the surface of the samples after 24 h in the salt spray environment. After 48 h in saline environment, a pit was formed in one of the SS3 coating and corrosion products were observed on the surface. It allowed the chloride contact with the magnesium alloy, causing the formation of $Mg(OH)_2$ (previously characterized in [28]) and damaging of the stainless steel coating. After 72 h in salt spray, new corroded zones appeared on the SS1, SS2 and SS3 coated surfaces. Nevertheless, for SS4 sample, no magnesium corrosion products were observed for any exposure time being protective until at least 72 h in chloride environments. This mechanism was also analyzed on the cross-section of the SS1 and SS4 samples (Figure 5). Figure 5a shows the cross-section of the SS1 sample, in which the presence of the corrosion products, and a pit with a depth of about 3 mm, demonstrate that chlorides penetrated the

coating, producing the corrosion of the magnesium alloy and the detachment of the coating. For the SS4 sample, the cross-sectional view demonstrated that the coating remained undamaged after the test (Figure 5b) and even no significative corrosion of the stainless steel coating was observed.

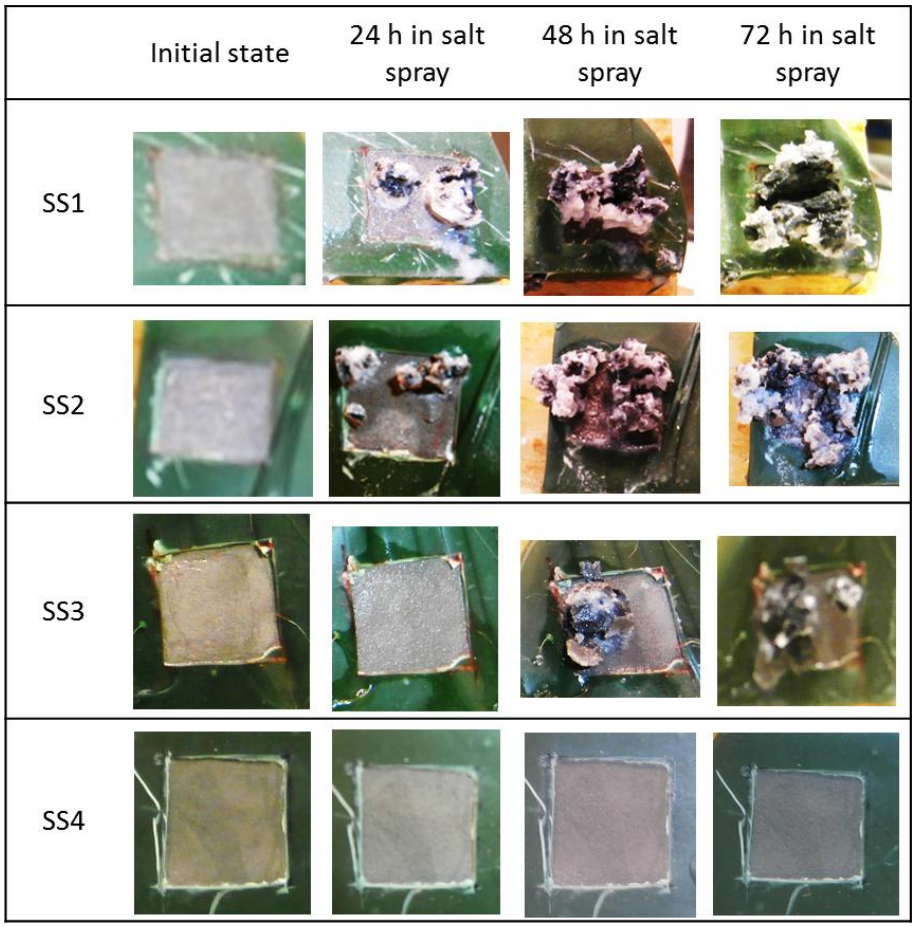

Figure 4. Surface morphology of the SS3 and SS4 samples before and after the corrosion test in the salt spray chamber.

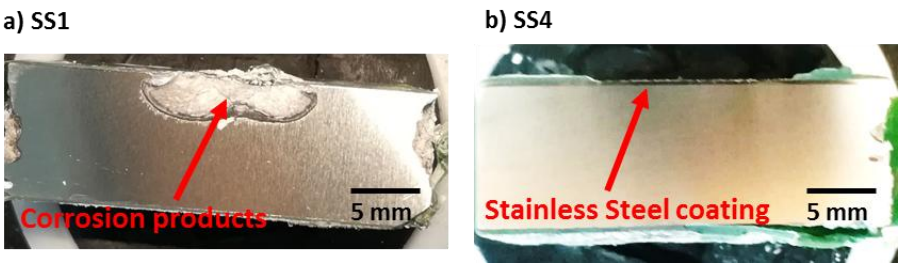

Figure 5. Cross-sectional view of a) SS1 and b) SS4 samples after the corrosion test in the salt-spray chamber.

3.4. Electrochemical impedance spectroscopy (EIS)

The Nyquist plots for the corrosion of ZE41 alloy in 3.5 wt.% NaCl solution at the different immersion times up to 144 h are shown in Figure 6a, the corresponding impedance modulus is plot in Figure 6b and the phase is plot in Figure 6c. The EIS spectra of the ZE41 magnesium alloy showed three defined loops. At the low frequency region, the inductive loop observed, which produces a change in the shape of the curves, is related to the adsorption process [2,34,35]. This inductive behavior could been ascribed to the presence of adsorbed metastable Mg^{+} on the metal surface or to the dissolution of the semi-passive corrosion product film. In the middle frequency region, the capacitive loop observed is attributed to the formation of a corrosion products layer and the diffusion of ions through it (mass transport). In the high frequency region, the capacitive loop observed is caused by the charge transfer reaction in the electric double layer formed at the interface between the Mg surface and the electrolyte. These two processes overlap, so it is difficult to distinguish them [36,37].

As observed in the Bode plot (Fig. 6b), the increase in the immersion time led to an increasement of the modulus of the impedance, where a maximum value was reached at 144 h of immersion time. This behavior is usually associated to the formation of a semi protective corrosion products film, as already has been observed by other authors for other magnesium alloys [38,39], which causes a reduction in the corrosion rate [40]. This behavior is in accordance with the *Rp* results obtained (Figure 3b) and, moreover, demonstrates the blocking effect of the oxides formed on the surface of the magnesium alloy.

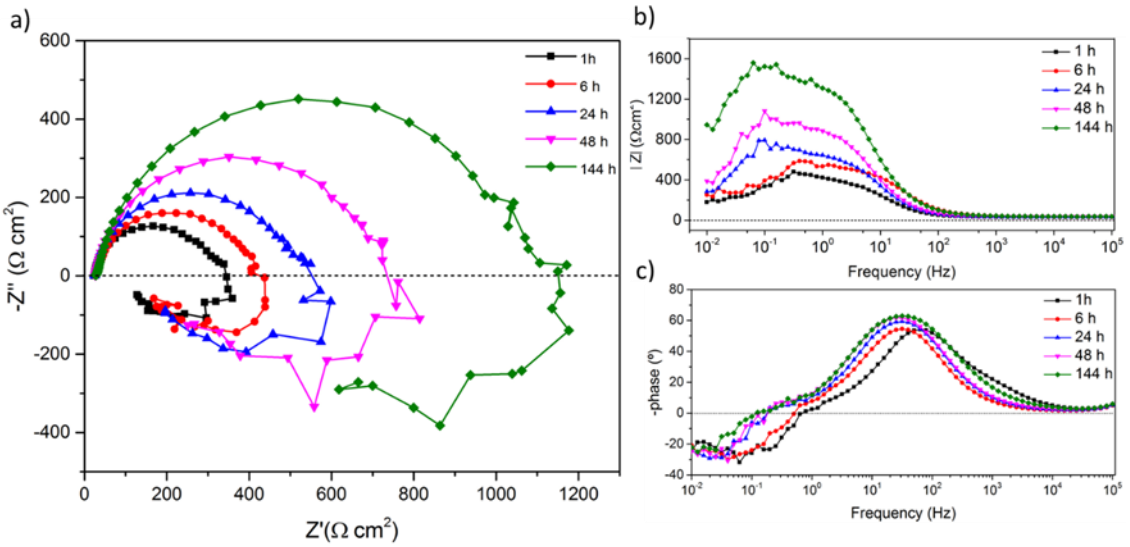

Figure 6. a) Nyquist and b) and c) Bode plots of the EIS spectra for the corrosion of ZE41 alloy.

Figure 7a shows the equivalent circuit used to fit the experimental data of ZE41 magnesium alloy where R_e is the resistance of the electrolyte, R_{cp} and CPE_{cp} are the resistance and the capacitive behavior of the corrosion products formed on the alloy substrate and R_{ct} and CPE_{dl} are the charge transfer resistance and the capacitance of the double layer corresponding to the electrochemical activities in the substrate/electrolyte interface [36]. R_L and L were introduced to account the inductive behavior and they indicated the existence of metastable Mg^+ during the dissolution of magnesium alloy substrate (the low frequency inductance loop) [37]. Other authors used this same model to explain the corrosion behavior of AZ31, the pure Mg and ZM21 alloy [34] and the ZrN/Zr coated AZ91 magnesium alloy [22]. Constant phase elements were used instead of the capacitors to take into account the non-homogeneity of the surface (roughness). As an example of the simulation results, Figure 7b shows the fit and the experimental data of the Nyquist plots for the corrosion of the ZE41 magnesium alloy after 144 h in the 3.5 wt.% NaCl using this equivalent circuit. The quality of the fitting for the different times tested is similar to the one shown.

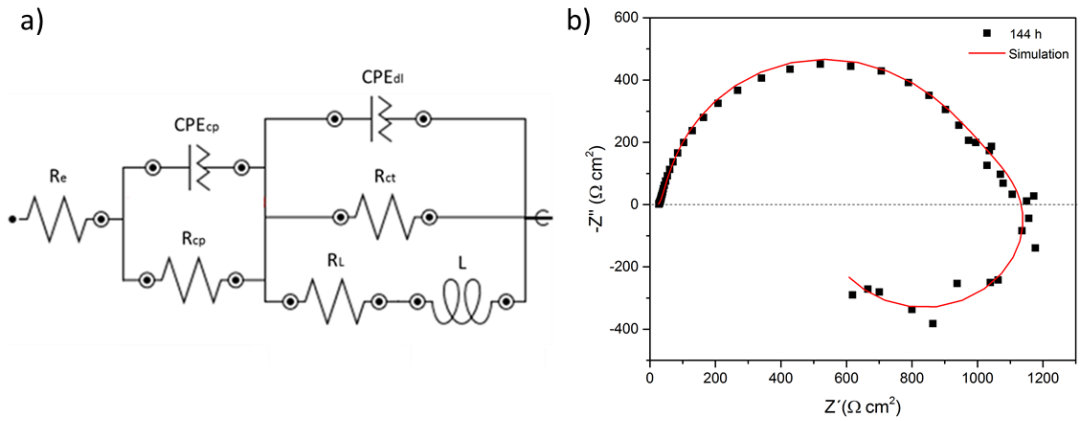

Figure 7. a) Equivalent circuit used to fit the EIS data for the ZE41 magnesium alloy substrate. b) Fitted and simulation data of the Nyquist plots for the corrosion of ZE41 after 144h in the electrolyte solution.

Table 4 and table 5 show the values of the electrochemical parameters obtained for the ZE41 magnesium alloy for the best fitting of the electrochemical impedance spectroscopy for different immersion times. As shown in table 4, the R_{cp} values, corresponding to the resistance of the corrosion products formed, increase with the increase of the immersion time from 11.4 Ωcm^2 for 1 h to 513.0 Ωcm^2 at 144 h. This increase means that the thickness and compactness of the corrosion layer formed increases with the increase of immersion time as its directly dependent with thickness. Moreover, in the same way, a decrease in the CPE_{cp} parameter (Table 5) may be attributing to the increase of the thickness of this layer as a capacity of a dielectric layer is inversely dependent on the width. The decrease of the CPE_{dl} value with the increase of the immersion time supposes an increasement of the stability of the double layer, which implies an increasement of the resistance of the charge transfer (R_{ct}). The *L* and R_L values are stable up to the highest immersion time. The marked change in these parameters indicates that a change in the corrosion mechanisms has taken place for the longest time. The corrosion evolution is conditioned by the dilution of the semi passive corrosion products layer that forms metastable Mg^+ in the surface of the samples. This agrees

with the presence of a thicker corrosion products layer that can partially protect the sample surface but that is not stable.

The equivalent resistance of the circuits fitted for very low frequencies has been calculated to compare the linear polarization tests (R_P) with the EIS tests. For the best fitting of each EIS curve, we have determined the near Direct Current resistance. The impedance of the inductive elements has been set to zero and the circuit has been considered open at the capacitive elements; then the equivalent resistance of the circuit is calculated (R_{DC}). The resistances obtained (Table 4) are in full accordance with the values obtained in the linear polarization test increasing with time after a first reduction for very short times, reaching the maximum resistance value (~500 Ωcm^2) at 144 h of immersion time in the electrolyte solution.

Table 4. EIS simulated resistance values of ZE41 magnesium alloys.

Immersion time (h)	R_e (Ωcm^2)	R_{cp} (Ωcm^2)	R_{ct} (Ωcm^2)	R_L (Ωcm^2)	R_{DC} (Ωcm^2)
1	24,1	11,4	387,6	199,1	167,1
6	26,1	18,8	298,7	114,8	127,9
24	23,9	64,9	430,2	109,4	176,0
48	26,0	167,2	646,0	134,5	304,5
144	24,9	513,0	798,0	7,6	545,5

Table 5. Electrochemical parameters for the ZE41 magnesium alloy EIS analysis.

Immersion time (h)	CPE_{cp} ($\mu F/cm^2$)	n	CPE_{dl} ($\mu F/cm^2$)	n	L (kH)
1	410,8	0,681	32,9	0,901	1,1
6	225,6	1	102,1	0,907	1,0
24	692,3	0,689	73,35	0,930	3,5
48	2880,0	0,530	48,3	0,932	1,1
144	949,0	0,515	28,7	1	7,0

The impedance values of the SS1, SS2 and SS3 coated samples at the lowest frequency (0.01 Hz), Figures 8 b, d and f, respectively, were similar to the values obtained for the uncoated ZE41 magnesium alloy. However, at this frequency the highest results were obtained for the SS4 sample, with an impedance value close to 32000 $\Omega \cdot cm^2$ after 1h in NaCl 3.5 wt.%, and a

value close to 7000 $\Omega \cdot cm^2$ after 144 h. This indicates that this coating has a high corrosion resistance.

All the systems show an important dependence with immersion time, as shown in the changes in their impedance spectra. In all cases, the impedance value decreased with immersion time. For SS1 sample (Figure 8a), a capacitive response was obtained indicating that the electrolyte was penetrating the coating and producing the chemical degradation of the substrate. At low-medium frequencies a relaxation processes appeared, which was caused by electrochemical activity on the metal/electrolyte interface, as it occurs in [41]. In this case, the properties of the layer as a barrier did not exist from the first hour in the electrolyte solution.

For the SS2, after 24 h of immersion time, only the lineal region attributed to the diffusion was observed. This implies that the coating inhibited the penetration of chlorides to the substrate. However, the radius of the loop decreased as immersion time increased (Figure 8c) indicating that a reduction in the polarization resistance is taking place. After 48 h in NaCl, a capacitive response was obtained as well as a reduction in the modulus of impedance (Figure 8d), showing that chloride ions could cross the coating and reached the substrate, evidencing the limit to the protection against corrosion of this coating. This same behavior was obtained for SS3 sample, but the modulus of impedance decreased after 24 h of immersion time.

For the SS4 coated sample, only the lineal region attributed to the diffusion mechanism was observed at all immersion times. After the first hour of immersion, as shown in Figure 8g, the slope slightly decreased, which is caused by a reduction in the polarization resistance. The theoretical radius of the loop of the SS4 is much larger than that obtained for ZE41 magnesium alloy. So, the presence of the SS4 coating produces a decrease in the corrosion rate of the ZE41 magnesium alloy, showing the effectiveness of the stainless steel coating as a protective barrier against corrosion.

Equivalent circuits used for the EIS analysis for coated specimens are shown in Figures 9 a and b depending on the number of layers and the immersion time. With respect to the circuit used to analyze the magnesium spectra, the response of the coating has been added by introducing R_{coat}/CPE_{coat}. The circuit shown in Figure 9a was used for SS4 sample at all immersion times and for SS3 and SS2 samples at 1 and 6 h of immersion time because only the region attributed to the diffusion was observed. The circuit in Figure 9b was used for SS3 and SS2 samples at the longest immersion times and for SS1 sample at all immersion times because a capacitive response was obtained because the electrolyte (in green) penetrates the coating (in orange) and its interface (in blue) and produces the chemical degradation of the substrate (in grey).

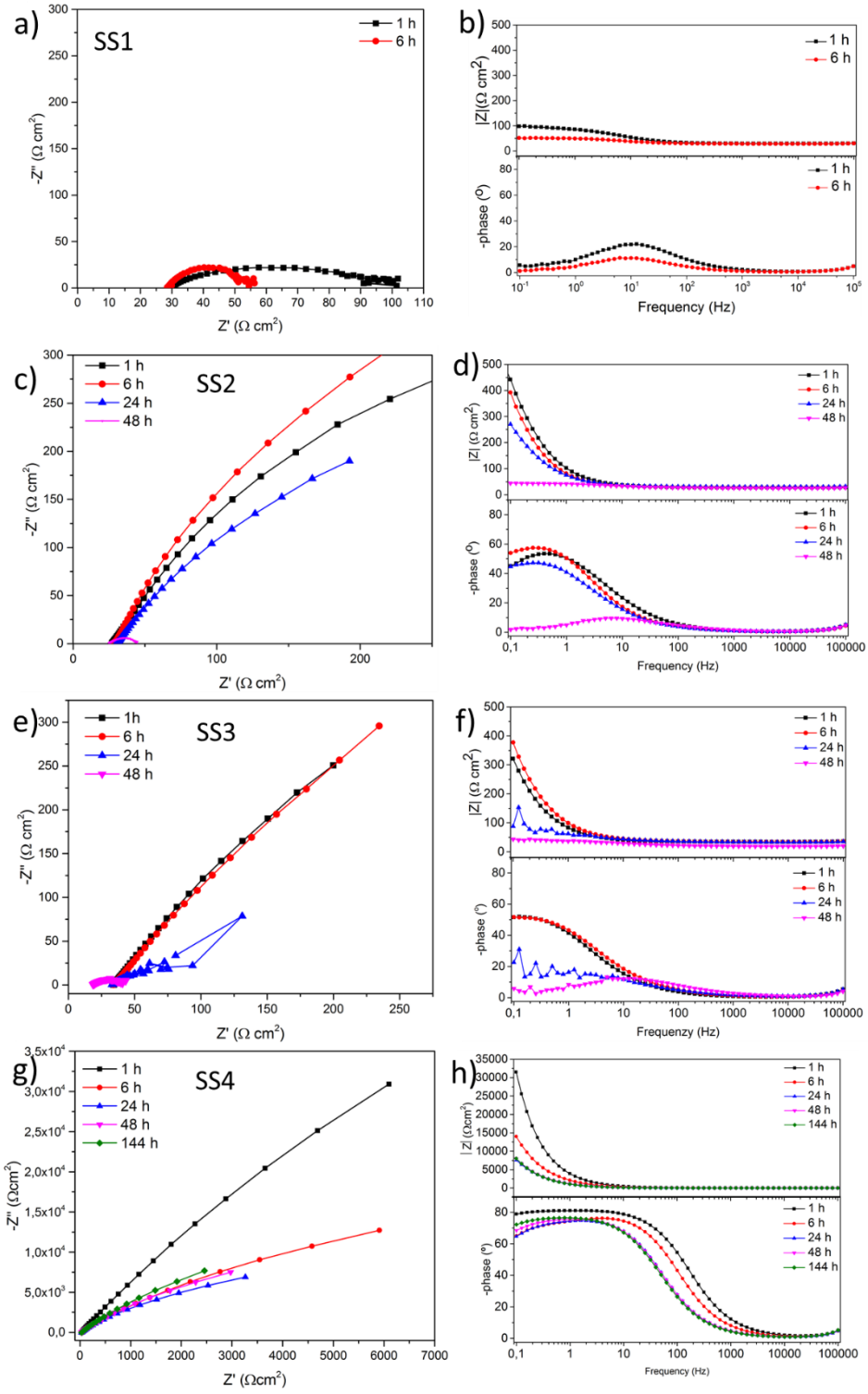

Figure 8. a) c) e) g) Nyquist and b) d) f) h) and Bode plots of the EIS spectra for the corrosion of each coated samples at different immersion times.

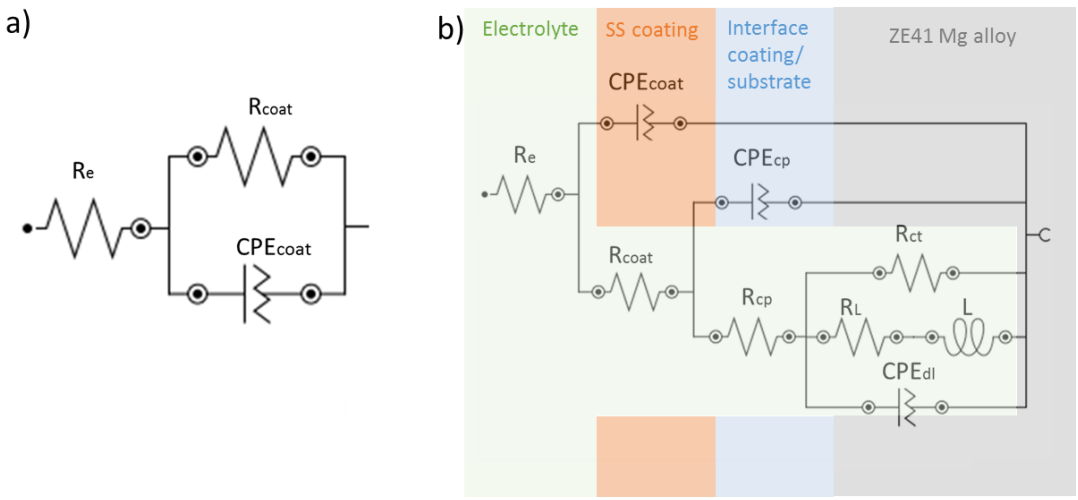

Figure 9. Equivalent circuits used to fit the EIS data for a) SS4 sample and SS3 and SS2 at low immersion times and b) SS3 and SS2 sample at high immersion times and SS1 sample.

The evolution of the coating corrosion resistance was analyzed by the changes in the values of R_{coat}, R_{cp} and R_{ct} (Figure 10). For all coatings the R_{coat} *and* R_{ct} values decreased with the increase of the immersion time. This progressive decrease indicates that the protective features of the coating reduce with the increase of the immersion time as a consequence of the electrolyte effect. Moreover, R_{coat} value increases with the increase of the number of layers of the coating, showing its maximum value for SS4 sample at 1 h of immersion time which indicates the higher corrosion resistance for this coating, as previous deduced from the potentiodynamic tests.

The analysis of the R_{coat} and CPE_{coat} obtained for the analysis of SS4 samples allows to determine the barrier properties of this coating (Figure 10d). When R_{coat} decreases and CPE_{coat} increases the protection ability of the coating decreases [42], as it occurs for this sample with the increase of the immersion time.

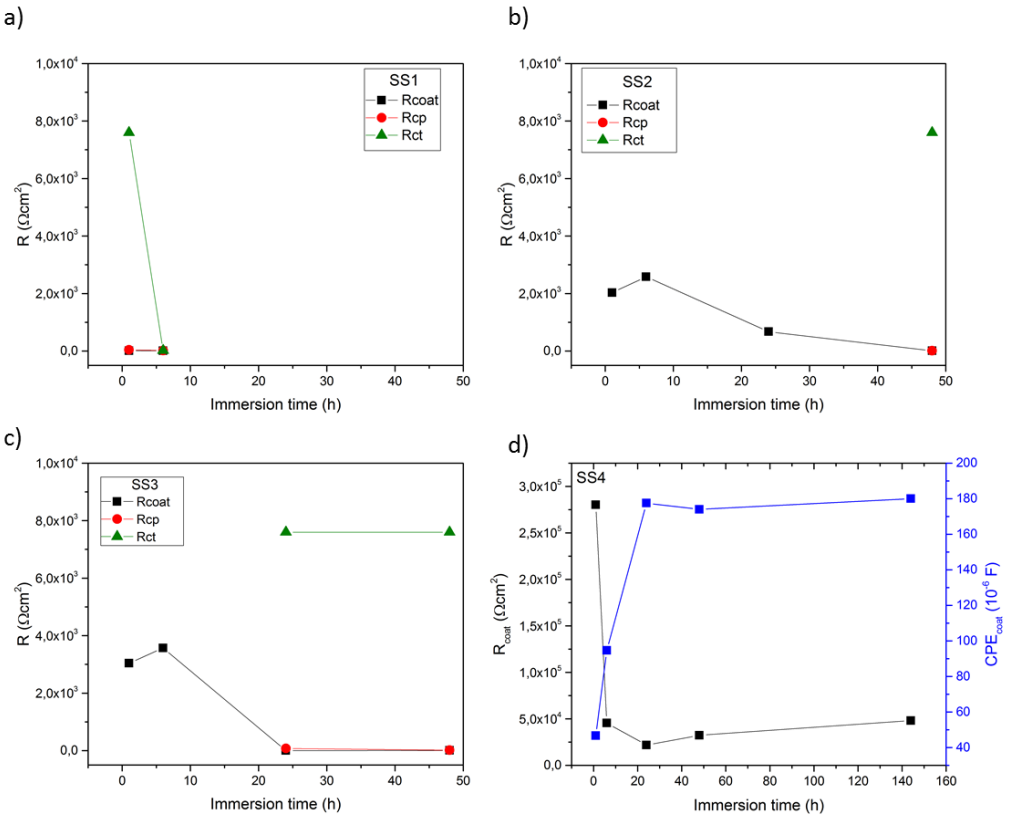

Figure 10. Evolution for the resistance for a) SS1, b) SS2, c) SS3 and d) SS4 samples.

3.5. Galvanic corrosion resistance

Due to the previous results, we also studied the galvanic corrosion of the SS4 stainless steel coating using the system shown in Figure 1, by exposing to a controllable salt spray environment in a chamber for 48 h and by immersion in 3.5 wt.% NaCl aqueous solution for 1 week. For comparative purposes, the same system was used to test ZE41 magnesium alloy and 316L stainless steel.

Figure 11 shows the surface morphology of ZE41, SS4 and 316L SS systems after the corrosion test in the salt spray chamber. An extensive corrosion occurs in the system form with uncoated ZE41 magnesium alloy after 48 h in a salt spray environment and white corrosion products appeared on the surface (Figure 11a). Thus, all the surface exposed to the salt-spray suffered corrosion.

Corrosion products were also obtained for 316L SS sample. The stainless steel sample corroded in a different way, as iron oxides were formed in the sample [43,44] (Figure 11c), indicating the oxidation of the sample instead of the corrosion of the galvanized nut and thread.

For the SS4 sample (Figure 11b), some white products were form around the screw, while the coating remained intact. The corrosion products deposited on the surface of the SS4 coated sample in the area that was near the screw during the test (Figure 12) were analyzed by EDX (Figure 12b), revealing the presence of ZnO. This indicates the preferential corrosion of the galvanized steel, which protected the stainless steel coating deposited, and that the Mg electrochemical corrosion is not taking place in this process.

Figure 13 shows the cross-section of the three samples. For ZE41 magnesium alloy some corrosion effects can be observed (marked by arrows). For 316L sample, no corrosion effect was observed. In the case of SS4 sample, the coating remaining without the presence of damage. A higher magnification of this is shown in Figure 14. The coating on the hole area is observed in Figure 14b and the corrosion products formed in the magnesium due to the penetration of the chlorides through the space between the sample and the screw. These white corrosion products formed were magnesium hydroxide ($Mg(OH)_2$) confirmed by the X-ray diffraction (Figure 14c) and previously characterized [28,45,46]. As shown the morphology of the coating remained intact after the test.

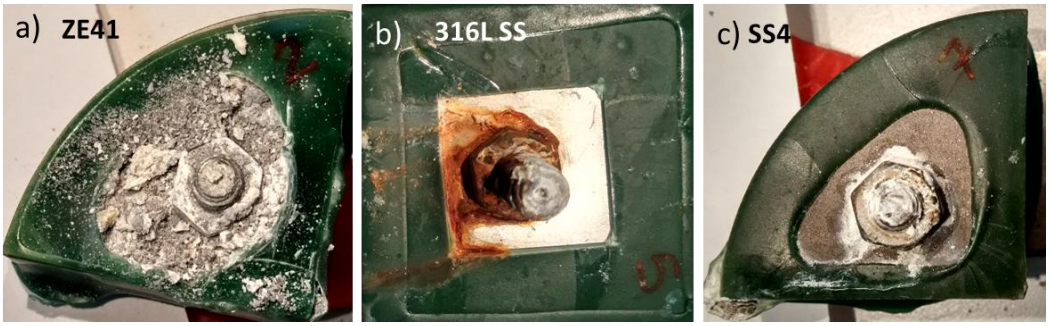

Figure 11. Surface morphology of a) ZE41 b) 316L SS and c) SS4 systems after the corrosion test in the salt spray chamber.

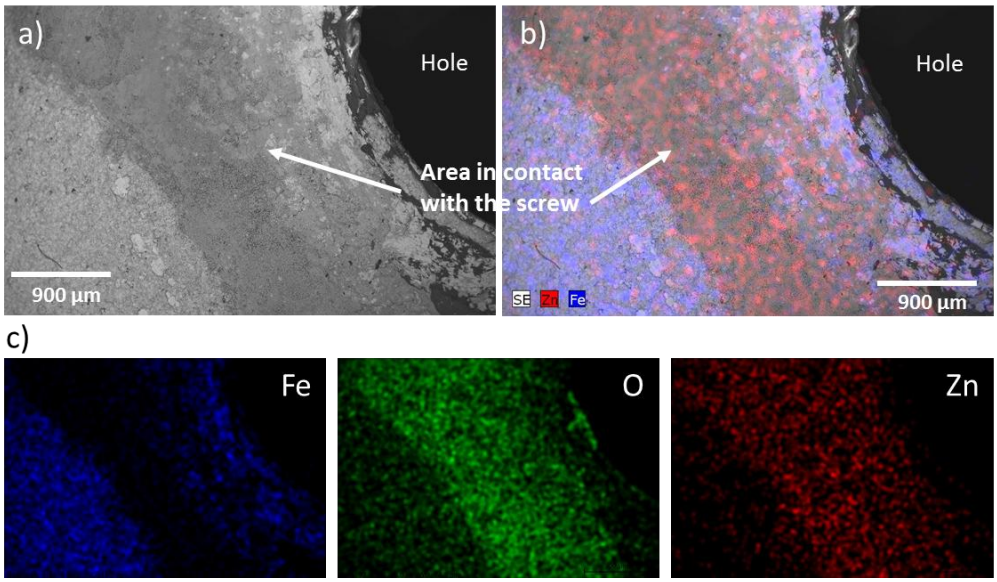

Figure 12. EDX analysis of the area in contact with the screw of the SS4 surface. a) SEM-BSE micrograph of the analyzed area, b) XRD map revealing Zn on the surface of the SS4 sample, c) Fe, O and Zn mappings.

Figure 13. Cross-section of ZE41, 316L and SS4 samples after the corrosion test in salt spray chamber.

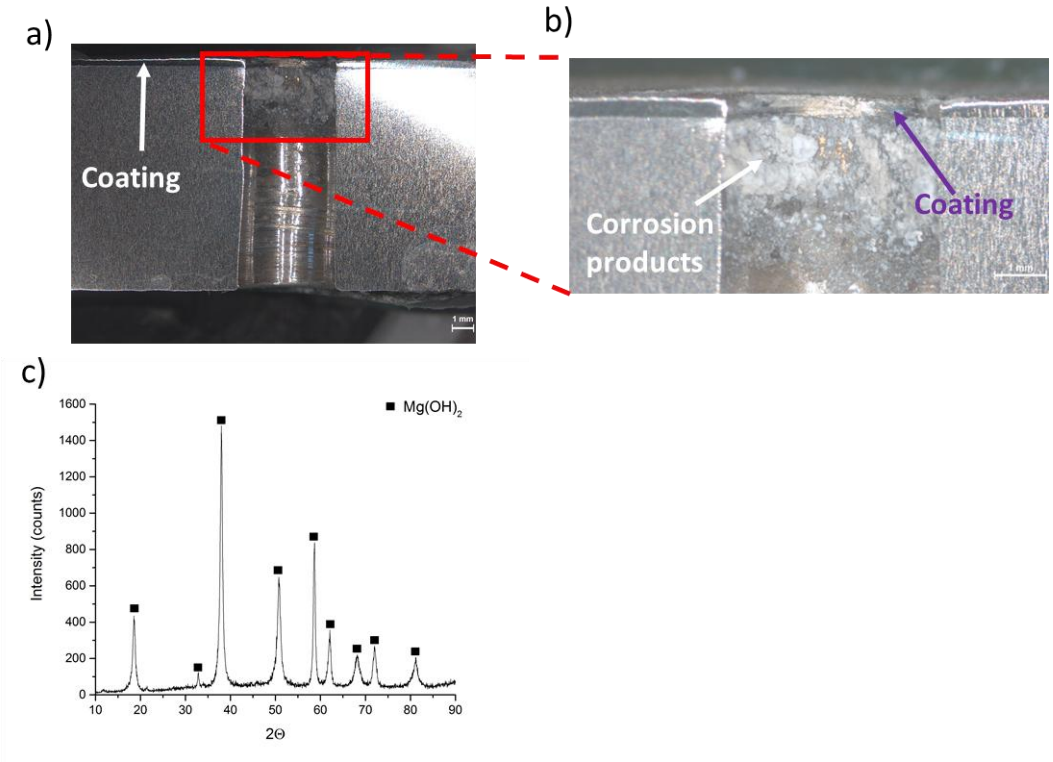

Figure 14. a) and b) Higher magnification of the cross-section of SS4 sample after the corrosion test and c) X-ray diffraction pattern of the white corrosion products.

These same systems were immersed in NaCl for one week. An area of 0.76 cm^2 included the screw and some of the sample surface was exposed to the medium. Figure 15 shows the macroscopic images for the three systems during the test. The corrosion for the uncoated magnesium alloy was much greater than that produced in the SS4 coating and in 316L SS. $Mg(OH)_2$ corrosion products were form on the screw. Figure 16 shows the macroscopic images of the samples after the immersion test and after removing the screw. Large corrosion was produced on the surface on ZE41 magnesium alloy (Figure 16a). The corrosion on the SS4 sample (Figure 16b) was located on the hole area, where the magnesium was in contact with the screw while the surface coated area remained intact (Figure 16c).

The cross-section of the SS4 sample (Figure 17b) showed the penetration of corrosion. Magnesium dissolution increased with depth and showed a maximum at 370 µm from the coating-substrate interface, for which the corrosion penetration was approximately 400 µm.

An image at higher magnifications of the coating (Figure 17c) shows that the top surface of the coating has not been affected by the corrosive process and that the corroded areas are located on the contact areas between the substrate and the screw. A magnification at other zone (Figure 17d) shows that there was little corrosion in the vicinity of the coating, as Mg remained attached to the steel coating. Below it, the zone where Mg was dissolved was filled with corrosion products, although they were brittle and some of them fell during sample preparation. These mechanisms evidence that the corrosion arouse because of the insufficient hermeticity of the thread used, as the zones that were most exposed to the solution did not show any corrosion. However, despite galvanic corrosion being limited, crevice corrosion was not avoided, and it caused the degradation of the Mg alloy substrate.

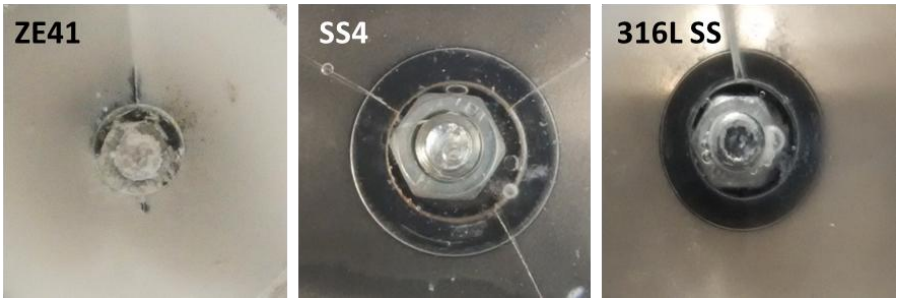

Figure 15. Macroscopic images during the immersion test in 3.5 wt.% NaCl medium of the ZE41, SS4 and 316L SS samples all in contact with a galvanized iron screw.

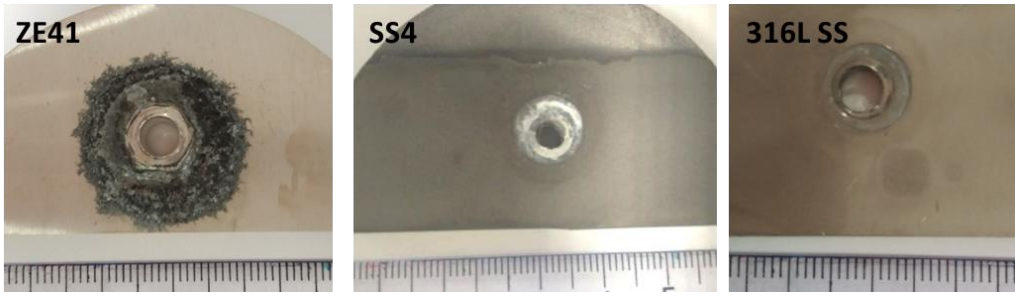

Figure 16. Macroscopic images after the immersion test in 3.5 wt.% NaCl medium of the ZE41, SS4 and 316L SS samples without the screw.

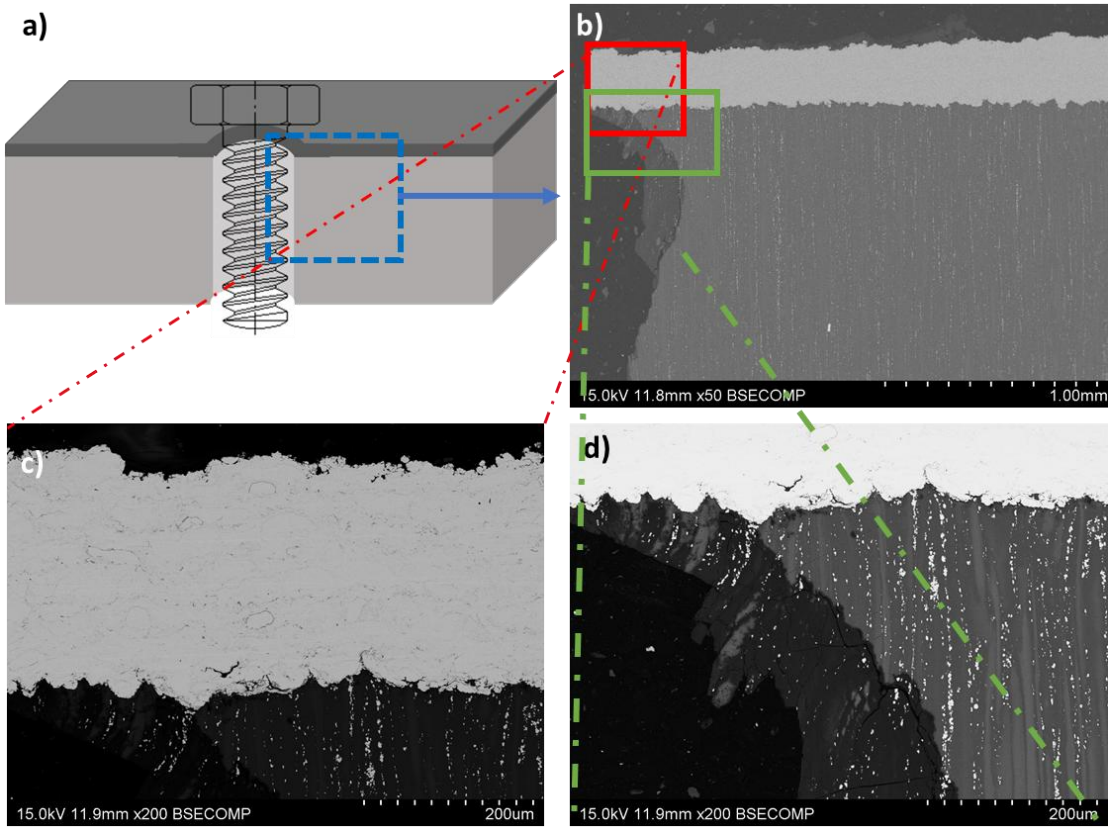

Figure 17. SEM-BSE micrographs of the cross-section of the SS4 sample after the immersion test in 3.5 wt.% NaCl.

To measure galvanic currents, galvanic couple was formed in a 3.5 wt.% NaCl solution by shortcutting the screw and the samples through an ammeter; the samples had the same size and SS4, ZE41 Mg alloy and 316L stainless steel samples were used.

The results showed an intensity of $2.01 \cdot 10^{-5}$ A for the SS4 coated sample and $1.20 \cdot 10^{-3}$ A for the magnesium alloy. The intensity in the SS4 sample was 60-fold lower that the intensity value obtained for the magnesium alloy, evidencing a strong reduction in the corrosion rate which reduced to $8.49 \cdot 10^{-10}$ mm/year for the SS4 sample. The intensity value obtained for the 316L stainless steel plate with the screw was $-9.24 \cdot 10^{-6}$ A for the 316L SS. This value is about half of the intensity of the SS4 sample and the negative sign indicates that corrosion takes

place in the plate and not in the screw, as it was previously suggested by the oxides formed in the different tests. Therefore, the SS4 coating does not only protect from generalized and localized corrosion but also prevents the presence of galvanic corrosion when this sample are in contact with galvanized steel parts.

4. Conclusions

Stainless steel coatings with different number of layer have been deposited on ZE41 magnesium alloy using optimized spraying parameters. All coatings were continuous, well adhered to the substrate and free of porosity. Increasing the number of layers increases the compactness of the coating and its hardness, which exceeded the nominal values of bulk stainless steels with similar composition.

The electrochemical results in 3.5 wt.% NaCl demonstrate the absence of diffusion across the SS4 coating even after 1 week immersion time. Coatings with lower number of layers detached from the substrates after 48 h for SS3 and 24 h for SS2 and SS1. Salt spray tests showed pitting corrosion SS1 and SS2 samples after 24 h of exposure time and after 48 h for the SS3 sample, while the SS4 coating remained intact after 72 h in salt spray environment. These differences were explained by the compactness, mechanical stability and defects present in the coatings.

The EIS tests in uncoated ZE41 Mg alloy have been fitted using an equivalent circuit. It shows that there was a growth in the modulus of its impedance and in its polarization resistance with a reduction of the capacitive contribution. This has been explained by the presence of a semi-protective oxide layer on the surface of the ZE41 Mg alloy that grows with immersion time and that reduce the corrosion progression. In the coated systems, the evolution of the equivalent circuit values was determined and the coating failure was recorded. The EIS result and the

equivalent circuits correlate with the *Rp* results. A very lower corrosion rate was obtained for the SS4 coating than for ZE41 magnesium alloy for all immersion times.

The galvanic corrosion of the SS4 sample was tested by contacting it with a galvanized screw. The results obtained showed that the coating prevented galvanic corrosion of the Mg substrate in salt-spray environment and in immersion.

Acknowledgements

Authors wish to thank Agencia Estatal de Investigación (Ministerio de Economía, Industria y Competitividad Project RTI2018-096391-B-C31) and Comunidad de Madrid (Project Aditimat S2018/NMT-4411).

Bibliography

[1] B.L. Mordike, T. Ebert, Magnesium Properties - applications - potential, Mater. Sci. Eng. A. 302 (2001) 37–45. doi:10.1016/S0921-5093(00)01351-4.

[2] Y. Zhang, C. Yan, F. Wang, W. Li, Electrochemical behavior of anodized Mg alloy AZ91D in chloride containing aqueous solution, Corros. Sci. 47 (2005) 2816–2831. doi:10.1016/J.CORSCI.2005.01.010.

[3] G.L. Makar, J. Kruger, Corrosion of magnesium, Int. Mater. Rev. 38 (1993) 138–153. doi:10.1179/095066093790326320.

[4] A.S. Gnedenkov, S.L. Sinebryukhov, D. V. Mashtalyar, S. V. Gnedenkov, Protective properties of inhibitor-containing composite coatings on a Mg alloy, Corros. Sci. 102 (2016) 348–354. doi:10.1016/j.corsci.2015.10.026.

[5] F. Cao, G.L. Song, A. Atrens, Corrosion and passivation of magnesium alloys, Corros. Sci. 111 (2016) 835–845. doi:10.1016/j.corsci.2016.05.041.

[6] R. Ambat, N.N. Aung, W. Zhou, Evaluation of microstructural effects on corrosion behaviour of AZ91D magnesium alloy, Corros. Sci. 42 (2000) 1433–1455. doi:10.1016/S0010-938X(99)00143-2.

[7] B.L.M. Hordt E. Friedrich, Magnesium Technology: Metallurgy, Design Data, Applications, 2006. doi:10.1007/3-540-30812-1_2.

[8] H. Huo, Y. Li, F. Wang, Corrosion of AZ91D magnesium alloy with a chemical conversion coating and electroless nickel layer, Corros. Sci. 46 (2004) 1467–1477. doi:10.1016/J.CORSCI.2003.09.023.

[9] A.J. López, J. Rams, A. Ureña, Sol–gel coatings of low sintering temperature for corrosion protection of ZE41 magnesium alloy, Surf. Coatings Technol. 205 (2011)

4183–4191. doi:10.1016/j.surfcoat.2011.03.011.

[10] C. Taltavull, B. Torres, A.J. Lopez, P. Rodrigo, E. Otero, A. Atrens, J. Rams, Corrosion behaviour of laser surface melted magnesium alloy AZ91D, Mater. Des. 57 (2014) 40–50. doi:10.1016/J.MATDES.2013.12.069.

[11] D. Zhang, B. Wei, Z. Wu, Z. Qi, Z. Wang, A comparative study on the corrosion behaviour of Al, Ti, Zr and Hf metallic coatings deposited on AZ91D magnesium alloys, Surf. Coatings Technol. (2016). doi:10.1016/j.surfcoat.2016.03.079.

[12] R. Arrabal, A. Pardo, M.C. Merino, M. Mohedano, P. Casajús, S. Merino, Al/SiC thermal spray coatings for corrosion protection of Mg–Al alloys in humid and saline environments, Surf. Coatings Technol. 204 (2010) 2767–2774. doi:10.1016/j.surfcoat.2010.02.030.

[13] H.S. Sidhu, B. Singh Sidhu, S. Prakash, The role of HVOF coatings in improving hot corrosion resistance of ASTM-SA210 GrA1 steel in the presence of Na2SO4–V2O5 salt deposits, Surf. Coatings Technol. 200 (2006) 5386–5394. doi:10.1016/J.SURFCOAT.2005.07.008.

[14] L. Fedrizzi, S. Rossi, R. Cristel, P.L. Bonora, Corrosion and wear behaviour of HVOF cermet coatings used to replace hard chromium, Electrochim. Acta. 49 (2004) 2803–2814. doi:10.1016/J.ELECTACTA.2004.01.043.

[15] G. Bolelli, V. Cannillo, L. Lusvarghi, R. Rosa, A. Valarezo, W.B. Choi, R. Dey, C. Weyant, S. Sampath, Functionally graded WC–Co/NiAl HVOF coatings for damage tolerance, wear and corrosion protection, Surf. Coatings Technol. 206 (2012) 2585–2601. doi:10.1016/J.SURFCOAT.2011.11.018.

[16] J.A. Picas, A. Forn, S. Menargues, G. Matthäus, Recubrimientos multicapa obtenidos por

proyecci{ó}n t{é}rmica HVOF, Catalu{ñ}a Dep. Cienc. Mater. e Ing. Met. Univ. Polit{é}cnica Catalu{ñ}a. (2004) 1–6.

[17] H. Herman, S. Sampath, R. McCune, Thermal spray: Current status and future trends, MRS Bull. 25 (2000) 17–25. doi:10.1557/mrs2000.119.

[18] J.M. Guilemany, J. Fernández, N. Espallargas, P.H. Suegama, A. V. Benedetti, Influence of spraying parameters on the electrochemical behaviour of HVOF thermally sprayed stainless steel coatings in 3.4% NaCl, Surf. Coatings Technol. 200 (2006) 3064–3072. doi:10.1016/j.surfcoat.2005.02.116.

[19] D. Zois, A. Lekatou, M. Vardavoulias, Preparation and characterization of highly amorphous HVOF stainless steel coatings, J. Alloys Compd. (2010). doi:10.1016/j.jallcom.2010.02.062.

[20] J.M. Guilemany, J. Fernández, J.M. De Paco, J. Sanchez, Corrosion resistance of HVOF WC-Co and TiC/Ni-Ti coatings sprayed on commercial steel, Surf. Eng. 14 (1998) 133–135. doi:10.1179/sur.1998.14.2.133.

[21] L. Zhao, E. Lugscheider, Influence of the spraying processes on the properties of 316L stainless steel coatings, Surf. Coatings Technol. 162 (2003) 6–10. doi:10.1016/S0257-8972(02)00560-1.

[22] Y. Xin, C. Liu, K. Huo, G. Tang, X. Tian, P.K. Chu, Corrosion behavior of ZrN/Zr coated biomedical AZ91 magnesium alloy, Surf. Coat. Technol. 203 (2009) 2554–2557. doi:10.1016/j.surfcoat.2009.02.074.

[23] N.R. Buenfeld, J.Z. Zhang, Impedance spectroscopy monitoring of a polyurethane coating on mortar exposed to NaCl solution, J. Mater. Sci. 35 (2000) 39–44. doi:10.1023/A:1004724128509.

[24] H. Duan, K. Du, C. Yan, F. Wang, Electrochemical corrosion behavior of composite coatings of sealed MAO film on magnesium alloy AZ91D, Electrochim. Acta. 51 (2006) 2898–2908. doi:10.1016/j.electacta.2005.08.026.

[25] A. Ghasemi, V.S. Raja, C. Blawert, W. Dietzel, K.U. Kainer, Study of the structure and corrosion behavior of PEO coatings on AM50 magnesium alloy by electrochemical impedance spectroscopy, Surf. Coatings Technol. 202 (2008) 3513–3518. doi:10.1016/j.surfcoat.2007.12.033.

[26] F. Mansfeld, S.L. Jeanjaquet, M.W. Kendig, An electrochemical impedance spectroscopy study of reactions at the metal/coating interface, Corros. Sci. 26 (1986) 735–742. doi:10.1016/0010-938X(86)90037-5.

[27] S.C. Chung, J.R. Cheng, S.D. Chiou, H.C. Shih, EIS behavior of anodized zinc in chloride environments, Corros. Sci. 42 (2000) 1249–1268. doi:10.1016/S0010-938X(99)00129-8.

[28] S. García-Rodríguez, A.J. López, B. Torres, J. Rams, 316L stainless steel coatings on ZE41 magnesium alloy using HVOF thermal spray for corrosion protection, Surf. Coatings Technol. 287 (2016) 9–19. doi:10.1016/j.surfcoat.2015.12.075.

[29] ASTM D4541 Standard Test Method for Pull-Off Strength of Coatings Using Portable Adhesion Testers, (n.d.).

[30] D. Zois, A. Lekatou, M. Vardavoulias, Preparation and characterization of highly amorphous HVOF stainless steel coatings, J. Alloys Compd. 504 (2010) S283–S287. doi:10.1016/J.JALLCOM.2010.02.062.

[31] C.-J. Li, W.-Y. Li, Deposition characteristics of titanium coating in cold spraying, Surf. Coatings Technol. 167 (2003) 278–283. doi:10.1016/S0257-8972(02)00919-2.

[32] S. García-Rodríguez, B. Torres, A.J. López, E. Otero, J. Rams, Characterization and

mechanical properties of stainless steel coatings deposited by HVOF on ZE41 magnesium alloy, Surf. Coat. Technol. 359 (2019) 73–84. doi:10.1016/j.surfcoat.2018.12.056.

[33] Z. Zeng, N. Sakoda, T. Tajiri, S. Kuroda, Structure and corrosion behavior of 316L stainless steel coatings formed by HVAF spraying with and without sealing, Surf. Coatings Technol. 203 (2008) 284–290. doi:10.1016/j.surfcoat.2008.09.011.

[34] M. Jamesh, S. Kumar, T.S.N. Sankara Narayanan, Corrosion behavior of commercially pure Mg and ZM21 Mg alloy in Ringer's solution - Long term evaluation by EIS, Corros. Sci. 53 (2011) 645–654. doi:10.1016/j.corsci.2010.10.011.

[35] G. Baril, C. Blanc, N. Pébère, AC Impedance Spectroscopy in Characterizing Time-Dependent Corrosion of AZ91 and AM50 Magnesium Alloys Characterization with Respect to Their Microstructures, J. Electrochem. Soc. 148 (2001) B489. doi:10.1149/1.1415722.

[36] M. Mohedano, B.J.C. Luthringer, B. Mingo, F. Feyerabend, R. Arrabal, P.J. Sanchez-Egido, C. Blawert, R. Willumeit-Römer, M.L. Zheludkevich, E. Matykina, Bioactive plasma electrolytic oxidation coatings on Mg-Ca alloy to control degradation behaviour, Surf. Coatings Technol. 315 (2017) 454–467. doi:10.1016/j.surfcoat.2017.02.050.

[37] Y. Song, D. Shan, R. Chen, F. Zhang, E.-H. Han, Biodegradable behaviors of AZ31 magnesium alloy in simulated body fluid, Mater. Sci. Eng. C. 29 (2008) 1039–1045. doi:10.1016/j.msec.2008.08.026.

[38] D. Mandal, S. Viswanathan, Effect of heat treatment on microstructure and interface of SiC particle reinforced 2124 Al matrix composite, Mater. Charact. 85 (2013) 73–81. doi:10.1016/j.matchar.2013.08.014.

[39] D. Ahmadkhaniha, M. Fedel, M.H. Sohi, A.Z. Hanzaki, F. Deflorian, Corrosion behavior of magnesium and magnesium – hydroxyapatite composite fabricated by friction stir processing in Dulbecco ' s phosphate buffered saline, Eval. Program Plann. 104 (2016) 319–329. doi:10.1016/j.corsci.2016.01.002.

[40] N. Dinodi, A.N. Shetty, Electrochemical investigations on the corrosion behaviour of magnesium alloy ZE41 in a combined medium of chloride and sulphate, J. Magnes. Alloy. 1 (2013) 201–209. doi:10.1016/j.jma.2013.08.003.

[41] M. Mohedano, B.J.C. Luthringer, B. Mingo, F. Feyerabend, R. Arrabal, P.J. Sanchez-Egido, C. Blawert, R. Willumeit-Römer, M.L. Zheludkevich, E. Matykina, Bioactive plasma electrolytic oxidation coatings on Mg-Ca alloy to control degradation behaviour, Surf. Coatings Technol. 315 (2017) 454–467. doi:10.1016/j.surfcoat.2017.02.050.

[42] L.C. Córdoba, M.F. Montemor, T. Coradin, Silane / TiO 2 coating to control the corrosion rate of magnesium alloys in simulated body fluid, Eval. Program Plann. 104 (2016) 152–161. doi:10.1016/j.corsci.2015.12.006.

[43] B. Jegdić, S. Polić-Radovanović, S. Ristić, A. Alil, Corrosion Processes, Nature and Composition of Corrosion Products on Iron Artefacts of Weaponry, Sci. Tech. Rev. 61 (2011) 50–56.

[44] J. Liang, A. Deng, R. Xie, M. Gomez, J. Hu, J. Zhang, C.N. Ong, A. Adin, Impact of flow rate on corrosion of cast iron and quality of re-mineralized seawater reverse osmosis (SWRO) membrane product water, Desalination. 322 (2013) 76–83. doi:10.1016/j.desal.2013.05.001.

[45] R. Arrabal, A. Pardo, M.C. Merino, S. Merino, M. Mohedano, P. Casajús, Corrosion behaviour of Mg/Al alloys in high humidity atmospheres, Mater. Corros. 62 (2011) 326–334. doi:10.1002/maco.200905538.

[46] S. Feliu, I. Llorente, Corrosion product layers on magnesium alloys AZ31 and AZ61: Surface chemistry and protective ability, Appl. Surf. Sci. 347 (2015) 736–746. doi:10.1016/j.apsusc.2015.04.189.